

Meteorological and soil surface effects in gamma radiation time series - implications for assessment of earthquake precursors

Susana Barbosa^a, Johan Alexander Huisman^b, Eduardo Brito Azevedo^c

^a*INESC TEC, CSIG - Centre of Information Systems and Computer Graphics, Portugal*

^b*Agrosphere Institute (IBG-3), Forschungszentrum Jlich GmbH, Juelich, Germany*

^c*Center of Climate Meteorology and Global Change, University of the Azores*

Abstract

Monitoring of environmental radioactivity for the purpose of earthquake prediction requires the discrimination of anomalies of non-tectonic origin from seismically-induced anomalies. This is a challenging task as time series of environmental radioactivity display a complex temporal pattern reflecting a wide range of different physical processes, including meteorological and surface effects. The present study is based on the detailed time series of gamma radiation from the Eastern North Atlantic (ENA) site in the Azores, and on very high resolution precipitation intensity and soil moisture time series. The results show that an abrupt shift in the average level of the gamma radiation time series previously reported as a potential earthquake precursor can also be explained by a corresponding abrupt change in soil moisture. It was concluded that the reduction of false positive earthquake precursors requires the detailed assessment of both precipitation and soil moisture conditions at high temporal resolution.

Keywords: gamma radiation, earthquakes, precipitation, soil moisture

1. Introduction

Radon (Rn-222) is considered a potential earthquake precursor based on diverse laboratory experiments showing that radon is released during rock fracturing (Holub & Brady, 1981; Mollo et al., 2011; Nicolas et al., 2014). It has also been shown that the connection of initially isolated cracks in crustal rocks before rupture can cause a release of radon transients measurable at the surface (Girault et al., 2017). However, the majority ($\sim 90\%$) of preseismic anomalies in radon concentration are not associated with seismic activity but rather with meteorological, hydrological, and environmental conditions (Jordan et al., 2011). Therefore, it is crucial for the application of radon as a geodynamic proxy to identify the origin of radon anomalies, which is a challenging task as anomalies of non-tectonic origin can be strikingly similar to seismo-tectonically induced radon anomalies (Woith, 2015; Arora et al., 2017).

The investigation of radon as a potential earthquake precursor requires long and continuous time series of field measurements. The long-term monitoring of Rn-222 at high temporal resolution can be performed using solid detectors or ionization chambers counting the alpha particles from radon decay, or alternatively by counting the gamma rays emitted by radon progeny. Crystal scintillators for gamma ray detection are advantageous for long-term monitoring in stable subsurface conditions due to their significantly higher capability to resolve temporal variations and ability to monitor directly short-term radon variations within the geological media, without the time delay required for the radon to move and reach equilibrium within the air volume sensed by the alpha detector (Zafir et al., 2011). Thus, gamma-ray detection systems can be useful for long-term monitoring for earthquake prediction purposes.

Anomalous variations in the temporal variability of gamma-ray counting rates have been reported preceding earthquake events (e.g. Tsvetkova et al. (2001, 2014); Fu et al. (2015); Novikov et al. (2016)). However, gamma radiation typically displays a complex temporal pattern, and equally strong variations can be also found in the absence of earthquakes. Thus, it is fundamental to

examine not only the association between anomalies in gamma radiation and
 32 earthquake events, but to also consider the whole temporal variability of gamma
 radiation and its relation to meteorological factors, including both atmospheric
 34 and surface effects. The temporal variability of gamma radiation is well known
 to be strongly influenced by precipitation (e.g. Inomata et al. (2007); Mercier
 36 et al. (2009); Bossew et al. (2017); Melintescu et al. (2018)) and by the soil
 water content (Carroll, 1981). A further influence is radon build-up within the
 38 stable boundary layer (e.g. Chambers et al. (2011)).

The present study illustrates the relevance of considering simultaneously
 40 meteorological and soil surface conditions when assessing potential earthquake
 precursory signs in gamma radiation time series. Based on a detailed record
 42 from the gamma radiation monitoring campaign at the Eastern North Atlantic
 (ENA) site in the Azores (Barbosa et al., 2017), this work focuses on a previ-
 44 ously reported potential earthquake precursor (Barbosa et al., 2016), and how
 it can actually be explained by a combination of very specific meteorological
 46 and surface conditions at the monitoring site.

2. Material and methods

48 2.1. Geographic setting

The Eastern North Atlantic (ENA) facility is a permanent ARM (Atmo-
 50 spheric Radiation Measurement) site installed at the Graciosa Island (39°N,
 28° W) of the Azores archipelago in the middle of the North Atlantic Ocean
 52 (Fig. 1). The location is unique from a geophysical point of view because it
 is located at the Azores triple junction of the Eurasian, North American, and
 54 African plates in a seismically and volcanically active area (Hildenbrand et al.,
 2014; Hipólito et al., 2014). The ENA station is located in the northern part
 56 of the Graciosa Island, situated in the northwestern tip of the slow-spreading
 Terceira rift separating the Eurasian plate to the North from the Nubian plate
 58 to the south (Vogt & Jung, 2004).

The climate of Graciosa is dictated by its geographical setting and its interaction with the surrounding sea, as well as by its size and altitude. From its position north of the central group of islands of the Azores, the island is very well exposed to the path of the intense meteorological activity that occurs along the Polar Front, crossing the archipelago by north from west to the east. The prevailing winds at the ENA site are also West-East. Due to its small dimension (only 61 square kilometers) and low altitude (only 402 meters high), the island does not interfere much with the marine boundary layer above, which led to the choice of Graciosa for the installation of the ENA facility (Nitschke & de Azevedo, 2015). According to the Köppen climate classification, the littoral climate of Graciosa is included in the temperate climates category with oceanic features (group Csb). It is characterized by having a summer and a winter, average annual temperature above 17°C, and annual average precipitation of 845 mm at sea level. Due to its lower altitude, Graciosa Island is one of the more sunny islands of the archipelago and also the one with less ability to produce orographic rain, making it one of the most driest islands of the Azores (Azevedo, 2015).

The soil of Graciosa reflects the volcanic origin of the island, being mainly derived from the evolution of tephra and basaltic rock in the mild and humid climate of the Atlantic (Madruga et al., 2015).

2.2. Monitoring set-up

Gamma radiation is continuously monitored at the ENA station since May 2015 in the framework of the Gamma Radiation Monitoring campaign. The gamma detector is a NaI(Tl) scintillator (Scionix, the Netherlands) equipped with an electronic total count Single Channel Analyzer (SCA) that detects gamma radiation in the energy range from 475 keV to 3 MeV in order to reduce the Compton background in the 50-475 keV low-energy range (Zafir et al., 2011). The sensor is installed inside a metal container at 1 m above ground with the scintillation head facing upwards.

88 2.3. Data

The gamma radiation data consist of a time series of total gamma-ray counts
90 with a 15-minute temporal resolution that has been collected since 2015/05/08
in counts per minute (cpm). The measurements were performed every 15-
92 minutes from May 2015 to April 2016, and then every 1-minute since May
2016. For consistency between the two measurement periods, the time se-
94 ries considered hereafter consists of 15-min counts from the 1st period and
the counts resulting from the temporal aggregation (sum) of the 1-min counts
96 from the 2nd period. The data is publicly available at the ARM archive
(<https://doi.org/10.5439/1441191>) and can be also freely obtained from a CKAN
98 repository (<https://rdm.inesctec.pt>).

Precipitation and soil moisture data are routinely measured at the ARM-
100 ENA facility, and they are freely available from the ARM data archive. Pre-
cipitation data are obtained from laser disdrometer measurements (Parsivel2,
102 Germany) every 1-minute. Soil moisture data is obtained from SEBS (Surface
Energy Balance System) measurements using a capacitive sensor (SMP1, Ra-
104 diation and Energy Balance Systems, Inc.) yielding soil water potential from
temperature-corrected resistance measurements. The soil water potential is fur-
106 ther converted to gravimetric soil moisture using a generic soil water charac-
teristic equation and assuming a very fine sandy loam as the soil type (Cook,
108 2016). The resulting values of soil moisture are available at 5 cm, 10 cm and
15 cm depths with a temporal resolution of 30 minutes. In this study, the soil
110 moisture time series are further re-scaled to an arbitrary range between 0 (dry)
and 1 (wet) corresponding to the daily minimum and maximum values of the
112 time series.

3. Results

114 3.1. Gamma radiation

The time series of gamma counts from the gamma monitoring campaign
116 at ENA is shown in Fig. 2 for the year 2015. The time series displays very

sharp peaks, typically lasting < 6 hours, which are more frequent and of higher
118 magnitude from mid-September to December. These sharp peaks are associated
with concurrent precipitation events (Barbosa et al., 2017) and result mainly
120 from the deposition of radon progeny, Pb-214 and Bi-214 (Livesay et al., 2014).

The time series of gamma counts shows an apparent break in the mean
122 level in mid-August 2015. The break is confirmed by the Mann-Whitney non-
parametric test for detecting shifts in the mean (Ross, 2015), which identifies
124 a small ($< 2\%$) but statistically significant change in the mean level of counts
from 7564 cpm to 7440 cpm on 26th August 2015 at 02h45 (vertical dashed
126 line in Fig. 2). Figure 3 shows a zoom of the time series of gamma counts
and precipitation rate around the identified breakpoint on 26th August. The
128 meteorological conditions are dominated by the passage of a frontal system with
strong precipitation occurring on August 26th from 00h00 to about 04h00. The
130 decrease in gamma radiation starts before the occurrence of the most intense
precipitation at 03h15, which seems to reduce the rate of decrease of gamma
132 counts. Strong precipitation is associated with enhanced radiation at ground
level as a result of precipitation scavenging of radon progeny (e.g. Paatero &
134 Hatakka (1999); Livesay et al. (2014); Yakovleva et al. (2016)), but in this case
the rain at 03:15 rather than enhancing seems to slow down the decrease in
136 gamma counts. While typically at the ENA site the enhancement in gamma
radiation resulting from strong precipitation is followed by lower counts due to
138 increased soil saturation (Barbosa et al., 2017), the effect typically lasts for some
hours after the rain event. In this case however the level of gamma radiation
140 remained lower than before the shift for several months, and relatively stable
until the end of the year, suggesting an alternative origin. The fact that an
142 earthquake occurred in the area at approximately the same time as the identified
shift in gamma radiation led to the suggestion that the shift in gamma radiation
144 could be associated with that seismic event (Barbosa et al., 2016).

3.2. Seismicity

146 Seismic information for the study area (31.5°W to 24.5°W , 36.5°N to 40.5°N)
is obtained from the EMSC (European-Mediterranean Seismological Centre)
148 catalog and from IPMA (Instituto Português do Mar e da Atmosfera) seismic
bulletins. All the earthquakes occurring in the region from the 8th of May to
150 December 31st, the period coincident with the gamma radiation monitoring in
2015, are selected from the catalogs and displayed in Figure 4. An earthquake
152 of magnitude ML3.3 (marked by an X in Fig. 4) occurred on 2015/08/26, the
same day as the level shift in gamma radiation. The earthquake happened at
154 02h16, about 30 minutes before the identified shift in the gamma radiation.
However, it is not the strongest event or the closest to the monitoring site. A
156 shallow event of the same magnitude (ML 3.3) and very near the location of the
earthquake of 26th of August occurred later (October 23th) with no apparent
158 change in the gamma radiation level.

Figure 5 shows the time series of gamma radiation (every 15-minutes) along
160 with precipitation intensity (every 1-minute) and wind information (wind direc-
tion and average wind speed) for the day of occurrence of the largest earthquake
162 events ($\text{ML} \geq 3.5$). The availability of very high temporal resolution precipita-
tion data allows to see clearly that the anomalies in gamma radiation before the
164 ML3.9 earthquake on May 8th 2015 and the ML3.6 earthquake on December
24th are related to intense precipitation and corresponding scavenging of radon
166 progeny. The strong precipitation in the evening of June 29th is of thermal
convection origin and thus not affects the gamma radiation counts (Barbosa
168 et al., 2017). Furthermore, the wind is predominantly blowing from the ocean
(NW direction) around this seismic event, which would have prevented eventual
170 radon transport from inland Graciosa. The ML4.2 and ML3.9 earthquakes on
June 14th, the ML4.0 earthquake on June 30th, the ML3.5 event on the 4th of
172 July and the ML4.5 event on September 26th are not associated with anomalies
in gamma radiation. Overall, there is little to no evidence for an association
174 between seismic events and gamma radiation anomalies for the considered earth-
quakes occurring in this area. This suggests that an alternative explanation for

176 the observed decrease in the level of gamma radiation after August 26th is
177 required.

178 3.3. Soil moisture

Soil water content is well known to influence gamma radiation measurements
180 via attenuation of the propagation of gamma rays from the subsurface (e.g.
Beamish (2013, 2015)). However, the influence of soil water content is considered
182 to be associated with long time scales, typically of several weeks and longer
(Minato, 1980; Yoshioka, 1994) and thus it seemed unlikely that an abrupt
184 variation as the one observed in gamma radiation on 26th August 2015 could
be related to soil moisture effects. However, the inspection of the available time
186 series of soil moisture from the ENA site (Figure 6) shows an abrupt change
from dry to wet conditions on August 26th 2015. This is confirmed by the
188 Mann-Whitney test for breakpoint detection, which identifies a shift in the soil
moisture time series at 5 cm and 10 cm depths on August 16th, and a day later
190 for soil moisture at the deeper level (15 cm). After the abrupt transition in
August from predominantly dry to wet conditions, the soil moisture remains
192 at a comparatively stable and higher level, which is consistent with the lower
average level of total gamma radiation until the end of 2015.

194 The relationship between daily-averaged soil moisture (at 5 cm) and gamma
radiation counts is displayed in Fig. 7. In order to remove the influence of
196 increased gamma radiation due to radon progeny on the ground due to rainfall,
the daily averages were computed from the 15-minute gamma radiation counts
198 by excluding all radiation measurements coincident and within 3 hours follow-
ing precipitation events with an intensity larger than 1 mm/hour. As expected,
200 higher soil moisture is associated with lower gamma counts, with a larger dis-
persion in the case of dry conditions. Although the relationship is nonlinear, as
202 indicated in Fig. 7 (dashed line) by the fitted local regression curve (Cleveland,
1979), a linear model seems nevertheless a fair approximation (solid line in Fig.
204 7). In fact, a simple linear regression is able to explain 66% of the variability
in daily gamma radiation as a function of daily soil moisture at 5 cm depth.

206 Figure 8 displays the time series of daily gamma radiation counts resulting from
the subtraction of counts associated with soil moisture as predicted from the
208 fitted linear model based on daily averaged soil moisture at 5 cm depth. This
time series corrected for atmospheric (precipitation > 1 mm/hour) and surface
210 (soil moisture) effects shows no sharp discontinuities.

4. Discussion

212 Diverse geoscience applications of gamma radiation measurements involve
the identification of anomalies that could be associated with the process of in-
214 terest, such as tectonic activity or fluid migration (Barbosa et al., 2015). It
is then crucial to identify confounding factors, such as meteorological effects
216 related to pressure and temperature (e.g. Zafrir et al. (2013)) or strong rainfall
events (e.g. Greenfield et al. (2002)). Understanding the anomalies in time se-
218 ries of environmental radioactivity is particularly critical for assessing potential
earthquake precursors. The task is hindered by the similarity of anomalies of
220 meteorological or hydrological origin and of anomalies of seismic origin, since
the underlying physical mechanism - mixing ratio change between different fluid
222 end-members driven by pressure changes in one end-member - can be the same
(Woith, 2015).

224 Soil moisture is well known to affect gamma radiation (e.g. Szegvary et al.
(2007); Stöhlker et al. (2012)), but typically the effect is expected to be approx-
226 imately linear and to take place on long time scales of weeks or longer. At the
ENA site, the temporal variability of soil moisture is strongly non-linear, with
228 very fast (< 1 day) transitions from dry to wet conditions. This pattern results
from the specific volcanic soil type and climatic conditions of the island. In the
230 flat northern platform of Graciosa island where the ENA station is located, the
soil thickness is typically small and porosity is high (Medina & Grilo, 1981).
232 The volcanic origin and sandy nature of the soil leads to high evaporation and
quick infiltration, resulting in the alternating behavior of soil moisture between
234 low values in the summer and high values in winter, with an abrupt transition

between the two states. In 2015, the transition from dry to wet conditions was
236 very abrupt and persisted in time (for several months) leading to a discontinuous
pattern in the time series of gamma radiation.

238 Soil moisture affects gamma radiation through the attenuation of photons
from terrestrial radionuclides, and thus gamma radiation measurements may re-
240 flect both sharp and slow soil moisture variations. Figure 9 shows the predicted
daily gamma radiation based on the linear relationship between gamma radia-
242 tion and soil moisture derived in section 3.4. Although the model is very simple,
it is able to capture the main features of the gamma radiation time series for
244 the year 2015 using only the available soil moisture information at 5 cm depth.
Fig. 9 also shows the predicted gamma radiation for the first-half of 2016 using
246 the same model. This provides an independent assessment of the performance
of the model since the parameters of the linear regression were estimated us-
248 ing only the gamma radiation and soil moisture measurements from 2015. The
predicted gamma radiation for 2016 agrees reasonably well with the observed
250 values in the first months of the year, but the predictions become progressively
worse after May 2016. This is hardly surprising since the model is very poor for
252 dry conditions, as indicated by the very large dispersion for low soil moisture in
Fig. 7. Nevertheless, the model predictions provide a very reasonable represen-
254 tation of long-term variability of gamma radiation for the winter period based
only on soil moisture at 5 cm depth for time scales of days to several weeks.

256 Figure 10 displays all the currently available soil moisture and gamma radi-
ation measurements from the ENA site (since May 2015 to the end of August
258 2018). Clearly, the seasonal variability of soil moisture is not fully reflected
in the gamma radiation measurements, although on average high soil moisture
260 values tend to be associated with lower gamma radiation. There are at least two
obvious reasons for this. First, near-surface gamma radiation not only depends
262 on terrestrial radiation from decaying radioisotopes within the soil, but is also
affected by cosmic radiation. At seasonal and longer time scales, variations in
264 background cosmic radiation need to be considered. Second, the vertical distri-
bution of soil moisture in the top soil needs to be considered since a single mea-

266 surement at 5 cm depth is likely not representative for the entire top soil affect-
 ing terrestrial gamma radiation. To make significant progress in understanding
 268 how soil moisture dynamics affects gamma radiation, a more elaborate modeling
 strategy combining depth-resolved hydrological models (Vereecken et al., 2015)
 270 and models for incoming and terrestrial gamma radiation would be needed,
 which is clearly beyond the scope of this manuscript.

272 It is important to emphasize that the obtained relationship between gamma
 radiation and soil moisture is site- and equipment-specific. As already shown
 274 by Beamish (2013), soil porosity is known to have a strong effect on this rela-
 tionship. More importantly, attenuation of gamma radiation by soil moisture
 276 is known to be energy-dependent, which means that the relationship between
 gamma radiation and soil moisture will depend on the measured energy spectra.
 278 Finally, the soil moisture measurements were normalized before further process-
 ing, which was necessary due to the rather primitive soil moisture sensors used
 280 at the ENA site (intended as a support to surface energy balance measurements
 rather than for the specific measurement of soil moisture). Future studies should
 282 consider the use of state-of-the-art soil moisture sensors, which are increasingly
 available at low cost (e.g. Bogen et al. (2017)).

284 5. Conclusions

The present study shows that abrupt changes in soil moisture can cause
 286 sharp variations in total gamma radiation measurements that can be confused
 with an earthquake precursory indicator. Therefore, soil moisture effects need
 288 to be taken into account to reduce the number of false positives in earthquake
 precursory studies (i.e., the cases when an anomaly exists but is not related to
 290 an earthquake event). It is thus fundamental to carefully assess not only me-
 teorological conditions, particularly precipitation, but also surface conditions,
 292 particularly soil moisture. High-resolution (sub-hourly) measurements of these
 parameters, as available at the ENA station, are critical to discriminate atmo-
 294 spheric and surface effects, as precipitation and soil moisture are not indepen-

dent and temporal averaging blurs the attribution of the sources of variability
in gamma radiation.

Acknowledgments

The invaluable technical assistance of Mr Carlos Sousa, Mr Bruno Cunha and Mr Tércio Silva from the ARM-ENA facility is gratefully acknowledged. Data were obtained from the Atmospheric Radiation Measurement (ARM) Program sponsored by the U.S. Department of Energy, Office of Science, Office of Biological and Environmental Research, Climate and Environmental Sciences Division. This work is partially supported by Project "Coral - Sustainable Ocean Exploitation: Tools and Sensors/NORTE-01-0145-FEDER-000036", financed by the North Portugal Regional Operational Programme (NORTE 2020) under the PORTUGAL 2020 Partnership Agreement and by the European Regional Development Fund (ERDF). Support from project POCI-01-0145-FEDER-006961 financed by the Operational Programme for Competitiveness and Internationalisation - COMPETE 2020, and National Funds through the FCT Fundação para a Ciência e a Tecnologia is also acknowledged.

References

- Arora, B. R., Kumar, A., Walia, V., Yang, T. F., Fu, C.-C., Liu, T.-K., Wen, K.-L., & Chen, C.-H. (2017). Assesment of the response of the meteorological/hydrological parameters on the soil gas radon emission at Hsinchu, northern Taiwan: A prerequisite to identify earthquake precursors. *Journal of Asian Earth Sciences*, 149, 49–63.
- Azevedo, E. (2015). O clima dos Açores - Projecto CLIMAAT - Centro do Clima, Meteorologia e Mudanças Globais da Universidade dos Açores. [Http://www.climaat.angra.uac.pt/](http://www.climaat.angra.uac.pt/).
- Barbosa, S., Donner, R., & Steinitz, G. (2015). Radon applications in geosciences - Progress & perspectives. *The European Physical Journal Special Topics*, 224, 597–603.

- Barbosa, S., Mendes, V. B., & Azevedo, E. B. (2016). Radon progeny monitoring
 324 at the Eastern North Atlantic (ENA), Graciosa island ARM facility and a
 potential earthquake precursory signal. In *EGU General Assembly Conference*
 326 *Abstracts* (p. 6270). volume 18.
- Barbosa, S., Miranda, P., & Azevedo, E. (2017). Short-term variability of
 328 gamma radiation at the {ARM} Eastern North Atlantic facility (Azores).
Journal of Environmental Radioactivity, 172, 218–231.
- 330 Beamish, D. (2013). Gamma ray attenuation in the soils of Northern Ireland,
 with special reference to peat. *Journal of Environmental Radioactivity*, 115,
 332 13–27.
- Beamish, D. (2015). Relationships between gamma-ray attenuation and soils in
 334 SW England. *Geoderma*, 259-260, 174–186.
- Bogena, H. R., Huisman, J. A., Schilling, B., Weuthen, A., & Vereecken, H.
 336 (2017). Effective calibration of low-cost soil water content sensors. *Sensors*,
 17, 208.
- 338 Bossew, P., Cinelli, G., Hernandez-Ceballos, M., Cernohlawek, N., Gruber, V.,
 Dehandschutter, B., Menneson, F., Bleher, M., Sthlker, U., Hellmann, I.,
 340 Weiler, F., Tollefsen, T., Tognoli, P., & de Cort, M. (2017). Estimating the
 terrestrial gamma dose rate by decomposition of the ambient dose equivalent
 342 rate. *Journal of Environmental Radioactivity*, 166, 296–308.
- Carroll, T. R. (1981). Airborne soil moisture measurement using natural ter-
 344 restrial gamma radiation. *Soil Science*, 132, 358–366.
- Chambers, S., Williams, A., Zahorowski, W., Griffiths, A., & Crawford, J.
 346 (2011). Separating remote fetch and local mixing influences on vertical radon
 measurements in the lower atmosphere. *Tellus B: Chemical and Physical*
 348 *Meteorology*, 63, 843–859.
- Cleveland, W. S. (1979). Robust Locally Weighted Regression and Smoothing
 350 Scatterplots. *Journal of the American Statistical Association*, 74, 829–836.

- Cook, D. R. (2016). Surface energy balance system (sebs) handbook. Doi: 10.2172/1245980.
- Fu, C.-C., Wang, P.-K., Lee, L.-C., Lin, C.-H., Chang, W.-Y., Giuliani, G., & Ouzounov, D. (2015). Temporal variation of gamma rays as a possible precursor of earthquake in the longitudinal valley of eastern taiwan. *Journal of Asian Earth Sciences*, 114, 362 – 372.
- Girault, F., Schubnel, A., & Pili, E. (2017). Transient radon signals driven by fluid pressure pulse, micro-crack closure, and failure during granite deformation experiments. *Earth and Planetary Science Letters*, 474, 409 – 418.
- Greenfield, M. B., Domondon, A. T., Okamoto, N., & Watanabe, I. (2002). Variation in -ray count rates as a monitor of precipitation rates, radon concentrations, and tectonic activity. *Journal of Applied Physics*, 91, 1628–1633.
- Hildenbrand, A., Weis, D., Madureira, P., & Marques, F. O. (2014). Recent plate re-organization at the Azores Triple Junction: Evidence from combined geochemical and geochronological data on Faial, S. Jorge and Terceira volcanic islands. *Lithos*, 210-211, 27–39.
- Hipólito, A., Madeira, J., Carmo, R., & Gaspar, J. a. L. (2014). Neotectonics of Graciosa island (Azores): a contribution to seismic hazard assessment of a volcanic area in a complex geodynamic setting. *Annals of Geophysics*, 56.
- Holub, R., & Brady, B. (1981). The effect of stress on radon emanation from rock. *Journal of Geophysical Research: Solid Earth*, 86, 1776–1784.
- Inomata, Y., Chiba, M., Igarashi, Y., Aoyama, M., & Hirose, K. (2007). Seasonal and spatial variations of enhanced gamma ray dose rates derived from ^{222}Rn progeny during precipitation in Japan. *Atmospheric Environment*, 41, 8043–8057.
- Jordan, T., Chen, Y.-T., Gasparini, P., Madariaga, R., Main, I., Marzocchi, W., Papadopoulos, G., Yamaoka, K., Zschau, J. et al. (2011). Operational

- 378 earthquake forecasting: State of knowledge and guidelines for implementation.
Annals of Geophysics, 54, 315–391.
- 380 Livesay, R., Blessinger, C., Guzzardo, T., & Hausladen, P. (2014). Rain-induced
 increase in background radiation detected by Radiation Portal Monitors.
 382 *Journal of Environmental Radioactivity*, 137, 137–141.
- Madrugá, J., Azevedo, E. B., Sampaio, J. F., Fernandes, F., Reis, F., & Pinheiro,
 384 J. (2015). Analysis and definition of potential new areas for viticulture in the
 Azores (Portugal). *SOIL*, 1, 515–526.
- 386 Medina, J. B., & Grilo, J. T. (1981). *Esboço pedológico da ilha Graciosa*
(Açores). Instituto Nacional de Investigação Científica.
- 388 Melintescu, A., Chambers, S., Crawford, J., Williams, A., Zorila, B., & Galeriu,
 D. (2018). Radon-222 related influence on ambient gamma dose. *Journal of*
 390 *Environmental Radioactivity*, 189, 67–78.
- Mercier, J.-F., Tracy, B., d’Amours, R., Chagnon, F., Hoffman, I., Korpach, E.,
 392 Johnson, S., & Ungar, R. (2009). Increased environmental gamma-ray dose
 rate during precipitation: a strong correlation with contributing air mass.
 394 *Journal of Environmental Radioactivity*, 100, 527–533.
- Minato, S. (1980). Analysis of Time Variations in Natural Background Gamma
 396 Radiation Flux Density. *Journal of Nuclear Science and Technology*, 17,
 461–469.
- 398 Mollo, S., Tuccimei, P., Heap, M., Vinciguerra, S., Soligo, M., Castelluccio, M.,
 Scarlato, P., & Dingwell, D. B. (2011). Increase in radon emission due to rock
 400 failure: An experimental study. *Geophysical Research Letters*, 38.
- Nicolas, A., Girault, F., Schubnel, A., Pili, É., Passelègue, F., Fortin, J., &
 402 Deldicque, D. (2014). Radon emanation from brittle fracturing in granites
 under upper crustal conditions. *Geophysical Research Letters*, 41, 5436–5443.

- 404 Nitschke, K., & de Azevedo, E. B. (2015). 3d atmosphere column evaluation
and clouds tomography: At eastern north atlantic (ena), graciosa island arm
406 facility. In *Experiment@ International Conference (exp. at'15), 2015 3rd* (pp.
91–92). IEEE.
- 408 Novikov, A., Ulin, S., Dmitrenko, V., Vlasik, K., Bychkova, O., Petrenko, D.,
Uteshev, Z., & Shustov, A. (2016). Measurement of radon concentration by
410 xenon gamma-ray spectrometer for seismic monitoring of the earth. *Journal
of Physics: Conference Series*, 675, 042007.
- 412 Paatero, J., & Hatakka, J. (1999). Wet deposition efficiency of short-lived radon-
222 progeny in central Finland. *Boreal Env. Res.*, 4, 285–293.
- 414 Ross, G. (2015). Parametric and Nonparametric Sequential Change Detection
in R: The cpm Package. *Journal of Statistical Software*, 66, 1–20.
- 416 Stöhlker, U., Bleher, M., Conen, F., & Bänninger, D. (2012). Harmonization of
ambient dose rate monitoring provides for large scale estimates of radon flux
418 density and soil moisture changes. *Proceedings Series*, (p. 53).
- Szegvary, T., Conen, F., Sthlker, U., Dubois, G., Bossew, P., & de Vries, G.
420 (2007). Mapping terrestrial gamma-dose rate in europe based on routine
monitoring data. *Radiation Measurements*, 42, 1561 – 1572.
- 422 Tsvetkova, T., Monnin, M., Nevinsky, I., & Perelygin, V. (2001). Research on
variation of radon and gamma-background as a prediction of earthquakes in
424 the caucasus. *Radiation Measurements*, 33, 1 – 5.
- Tsvetkova, T., Nevinsky, I., & Nevinsky, V. (2014). Results of spectral mon-
426 itoring of environmental gamma background in a fault zone of the western
caucasus for seismological application. *Radiation Measurements*, 69, 35 – 49.
- 428 Vereecken, H., Huisman, J.-A., Franssen, H. H., Brüggemann, N., Bogaen, H. R.,
Kollet, S., Javaux, M., van der Kruk, J., & Vanderborght, J. (2015). Soil hy-
430 drology: Recent methodological advances, challenges, and perspectives. *Wa-
ter resources research*, 51, 2616–2633.

- 432 Vogt, P., & Jung, W. (2004). The terceira rift as hyper-slow, hotspot-dominated
oblique spreading axis: a comparison with other slow-spreading plate bound-
434 aries. *Earth and Planetary Science Letters*, 218, 77–90.
- Woith, H. (2015). Radon earthquake precursor: A short review. *The European*
436 *Physical Journal Special Topics*, 224, 611–627.
- Yakovleva, V. S., Nagorsky, P. M., Cherepnev, M. S., Kondratyeva, A. G., &
438 Ryabkina, K. S. (2016). Effect of precipitation on the background levels of
the atmospheric beta- and gamma-radiation. *Applied Radiation and Isotopes*,
440 118, 190–195.
- Yoshioka, K. (1994). Study of Time Variation of Terrestrial Gamma Radiation
442 Due to Depth Distribution of Soil Moisture Content. *Radioisotopes*, 43, 183–
189.
- 444 Zafrir, H., Barbosa, S. M., & Malik, U. (2013). Differentiation between the
effect of temperature and pressure on radon within the subsurface geological
446 media. *Radiation Measurements*, 49, 39–56.
- Zafrir, H., Haquin, G., Malik, U., Barbosa, S., Piatibratova, O., & Steinitz,
448 G. (2011). Gamma versus alpha sensors for Rn-222 long-term monitoring in
geological environments. *Radiation Measurements*, 46, 611–620.

450 **List of figures**

Figure 1: Geographical location of the gamma radiation monitoring campaign at the Graciosa Island, Azores (top) and detail of the Eastern North Atlantic (ENA) ARM site (bottom). Soil moisture is obtained from SEBS (Surface Energy Balance System) measurements, at a distance of 130m from the gamma measurements.

452 **Figure 2:** Time series of total gamma counts in counts per minute (cpm), every 15 minutes from 2015-05-08 to 2015-12-31. The vertical dashed line marks
458 the time of the shift in the time series as identified by the Mann-Whitney test.

Figure 3: Detail of the time series of gamma counts (in cpm) and precipitation rate (in mm/hour) for the period around the identified break-point on 2015/08/26 02:45. Wind information (mean speed and wind direction) is
460 displayed for the same period on the top right.
462

Figure 4: Map with the locations of all earthquakes in the Azores region from 2015/05/08 to 2015/12/31. The ML3.3 earthquake on 2015/08/26 is marked by an X.
464

466 **Figure 5:** Detail of the time series of gamma counts (in cpm) and precipitation rate (in mm/hour) around the largest earthquake events (the dashed vertical line indicates the time of occurrence of the earthquake). Wind information (mean speed and wind direction) is shown on the top left side.

470 **Figure 6:** Time series of soil moisture values every 30-minutes (points) and daily averaged (black line) at 5cm (top), 10 cm (middle) and 15 cm (bottom) depths.
472

Figure 7: Scatter-plot of daily values of soil moisture (at 5 cm depth) and gamma radiation for the year 2015. The daily averages are computed excluding all the measurements coincident and within the following 3 hours of precipitation events with intensity larger than 1 mm/hour.
476

Figure 8: Time series of daily gamma counts after correction for the soil moisture influence using the fitted linear model (solid dark line) superimposed on the original time series of gamma measurements as in Fig. 2 (gray).
478

480 **Figure 9:** Time series of daily soil moisture (top) and gamma counts (bot-
tom, grey) along with gamma counts from the fitted linear model for the year
482 2015 (solid line, dark blue) and predictions from the model for the first half of
2016 (dashed line, light blue).

484 **Figure 10:** Time series of weekly averaged soil moisture (top) and gamma
counts (bottom) from May 2015 to the end of August 2018.

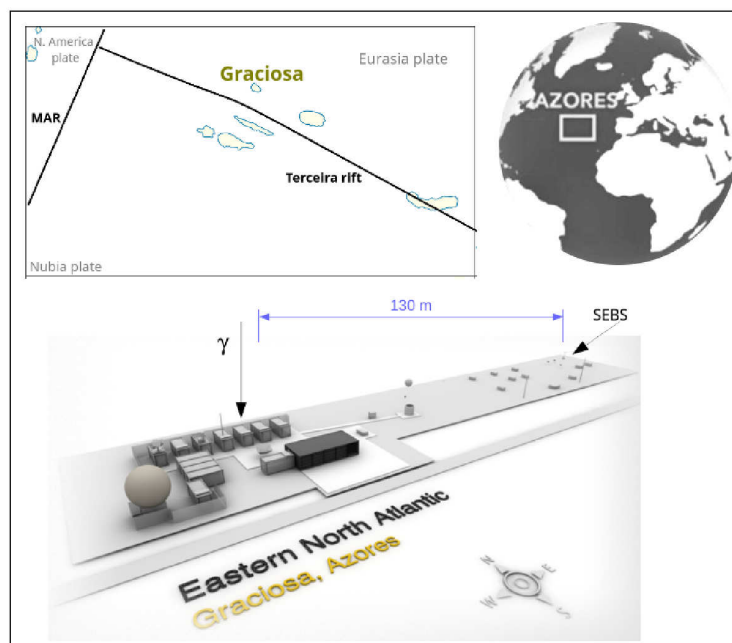


Figure 1: Geographical location of the gamma radiation monitoring campaign at the Graciosa Island, Azores (top) and detail of the Eastern North Atlantic (ENA) ARM site (bottom). Soil moisture is obtained from SEBS (Surface Energy Balance System) measurements, at a distance of 130m from the gamma measurements.

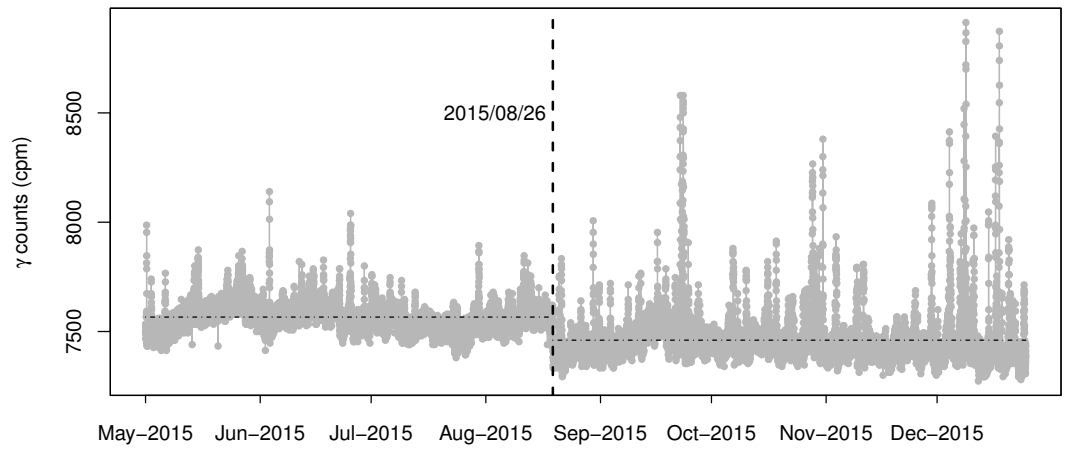


Figure 2: Time series of total gamma counts in counts per minute (cpm), every 15 minutes from 2015-05-08 to 2015-12-31. The vertical dashed line marks the time of the shift in the time series as identified by the Mann-Whitney test.

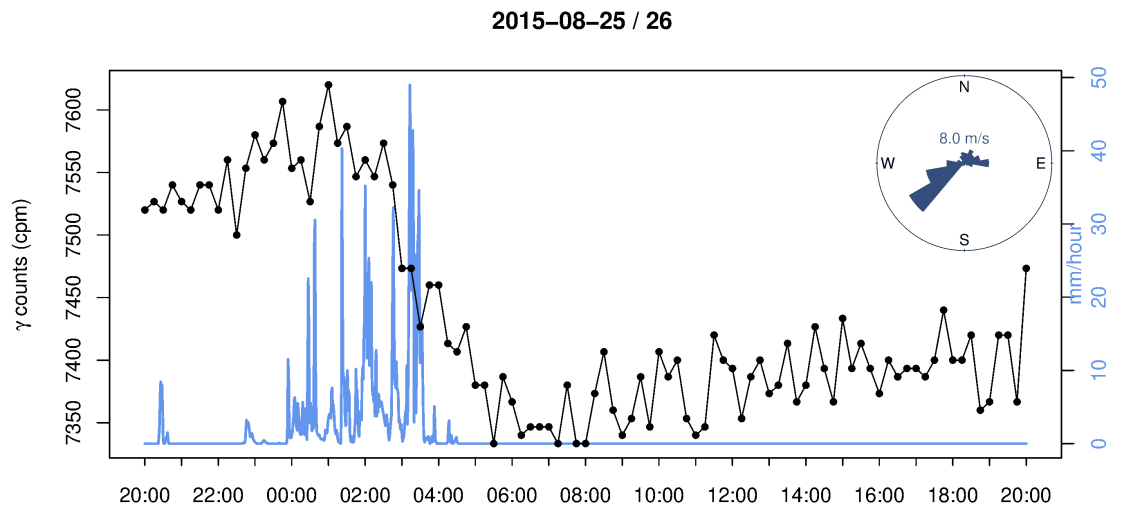


Figure 3: Detail of the time series of gamma counts (in cpm) and precipitation rate (in mm/hour) for the period around the identified break-point on 2015/08/26 02:45. Wind information (mean speed and wind direction) is displayed for the same period on the top right.

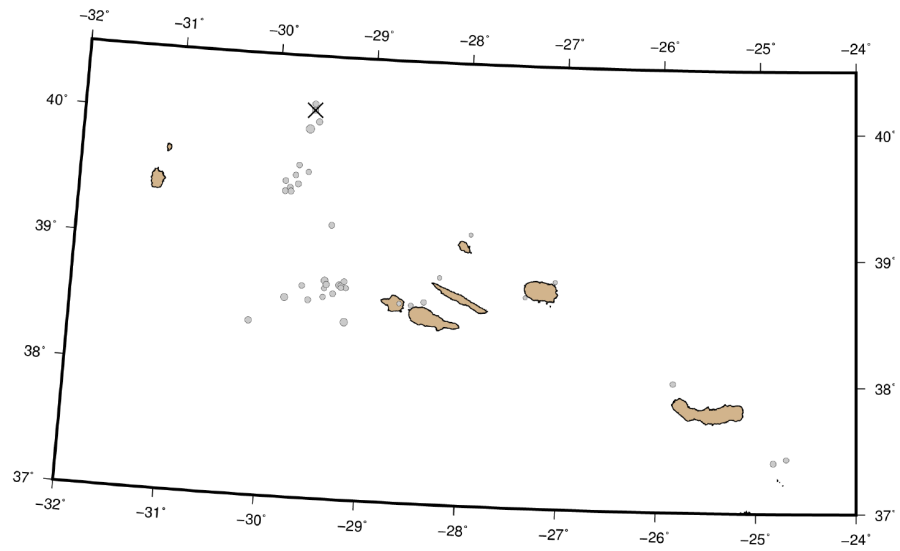


Figure 4: Map with the locations of all earthquakes in the Azores region from 2015/05/08 to 2015/12/31. The ML3.3 earthquake on 2015/08/26 is marked by an X.

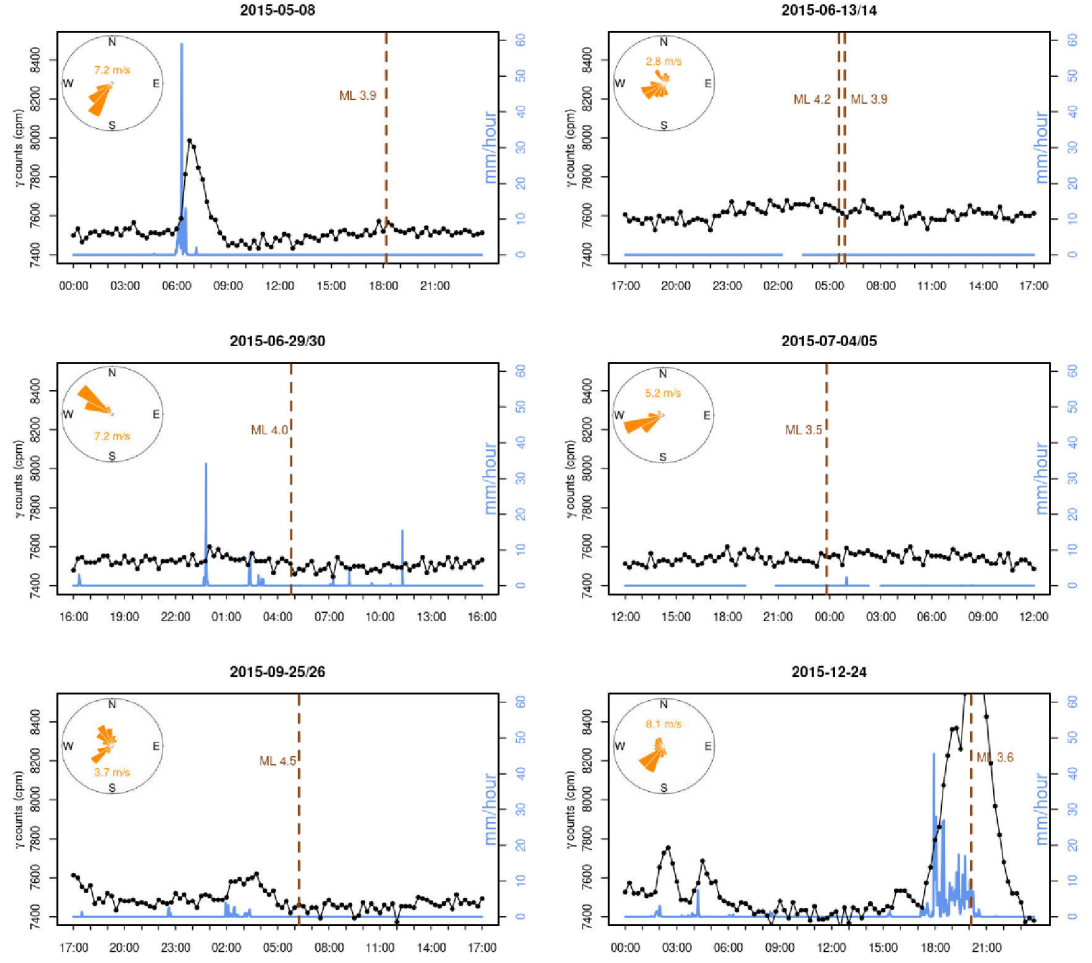


Figure 5: Detail of the time series of gamma counts (in cpm) and precipitation rate (in mm/hour) around the largest earthquake events (the dashed vertical line indicates the time of occurrence of the earthquake). Wind information (mean speed and wind direction) is shown on the top left side.

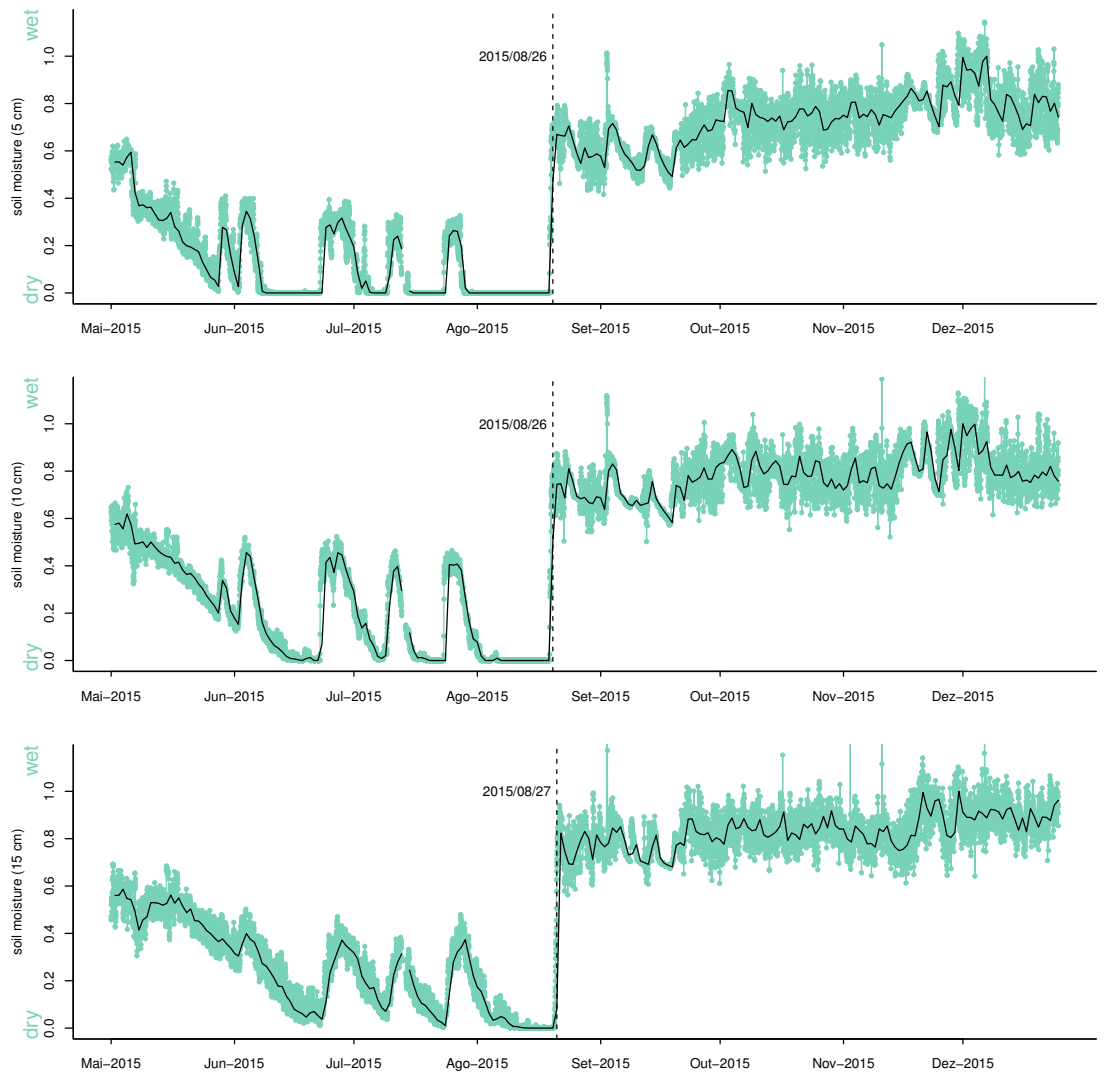


Figure 6: Time series of soil moisture values every 30-minutes (points) and daily averaged (black line) at 5cm (top), 10 cm (middle) and 15 cm (bottom) depths.

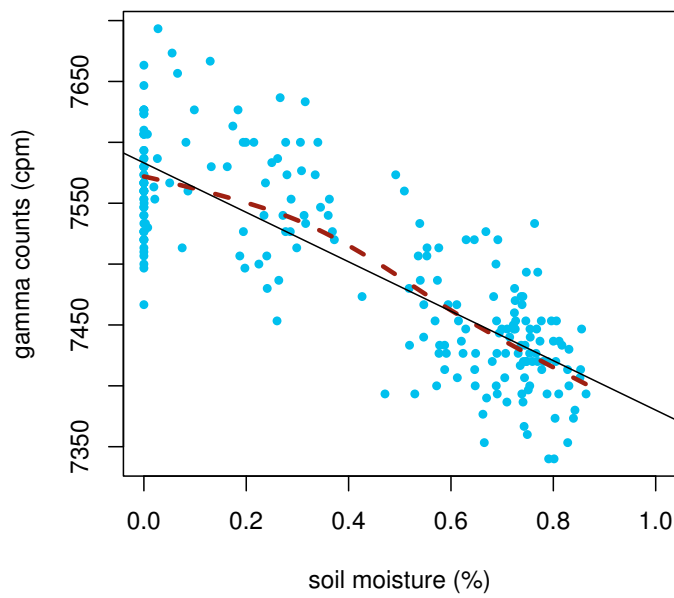


Figure 7: Scatter-plot of daily values of soil moisture (at 5 cm depth) and gamma radiation for the year 2015. The daily averages are computed excluding all the measurements coincident and within the following 3 hours of precipitation events with intensity larger than 1 mm/hour.

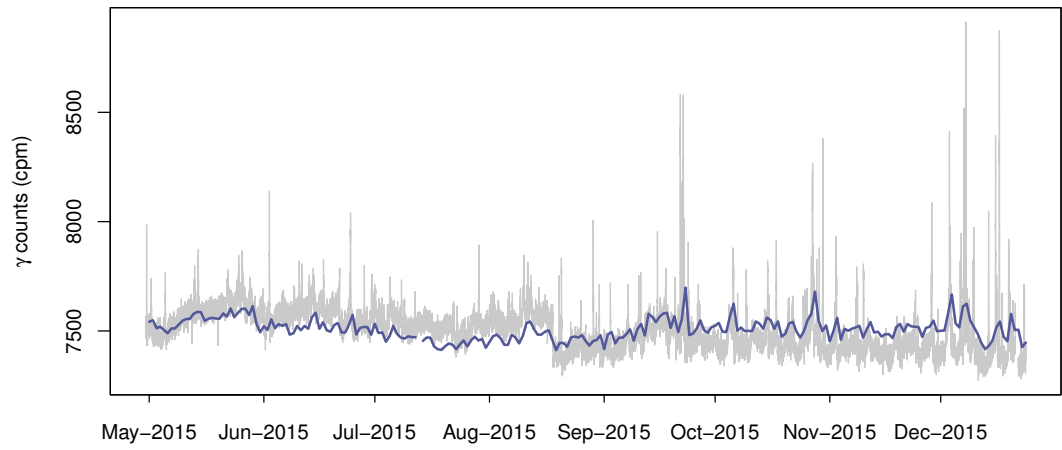


Figure 8: Time series of daily gamma counts after correction for the soil moisture influence using the fitted linear model (solid dark line) superimposed on the original time series of gamma measurements as in Fig. 2 (gray).

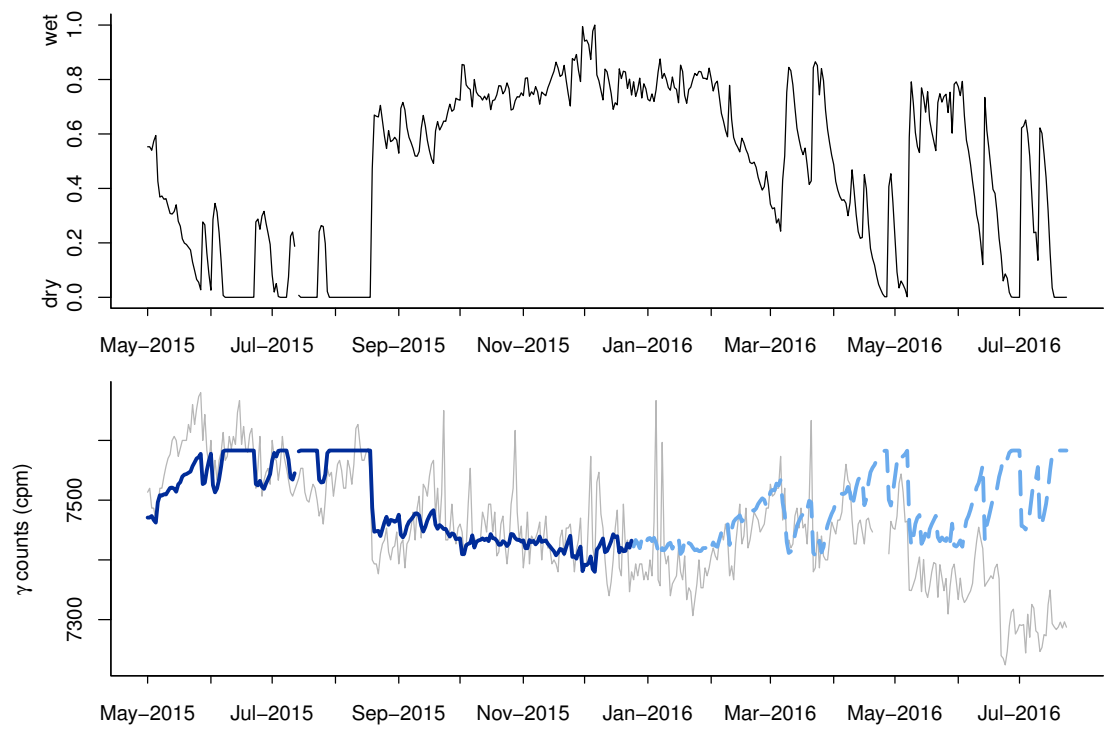


Figure 9: Time series of daily soil moisture (top) and gamma counts (bottom, grey) along with gamma counts from the fitted linear model for the year 2015 (solid line, dark blue) and predictions from the model for the first half of 2016 (dashed line, light blue).

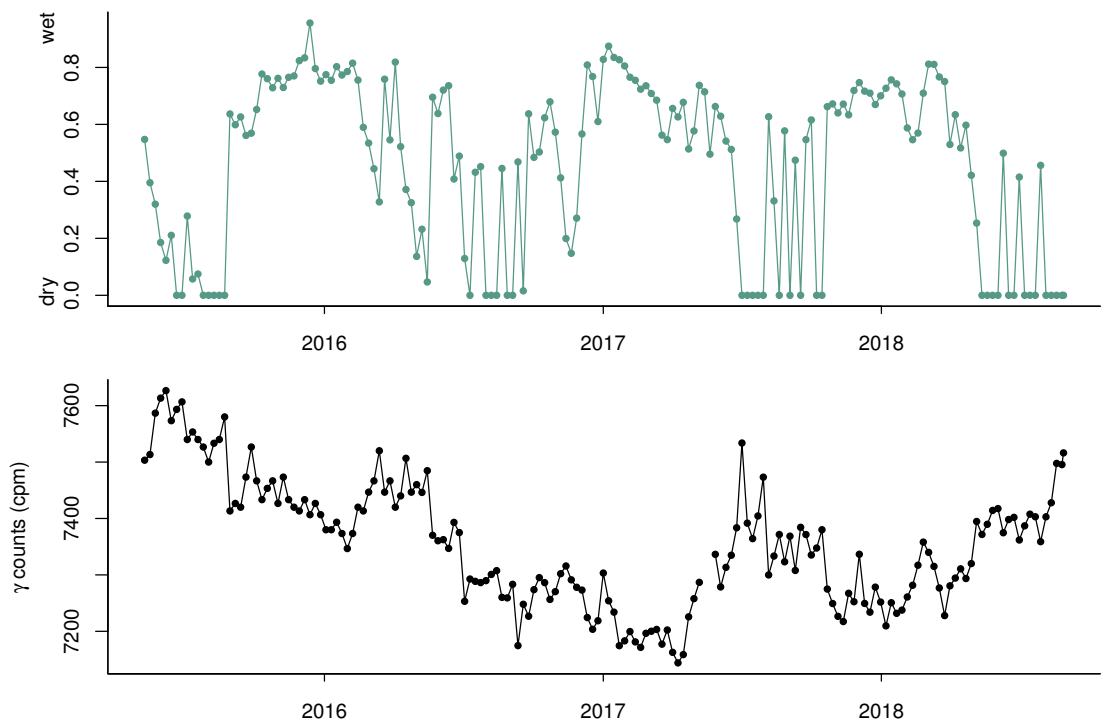


Figure 10: Time series of weekly averaged soil moisture (top) and gamma counts (bottom) from May 2015 to the end of August 2018.